Efficacy and safety of glycosphingolipid SSEA-4 targeting CAR-T cells in solid tumors

Monzo HJ[1*], Hyytiäinen M[1*], Elbasani E[1#], Kalander K[1,2#], Wall J[2], Moyano-Galceran L[3], Tanjore-Ramanathan J[1], Jukonen J[1], Laakkonen P[1,4], Ristimäki A[2,5], Carlson JW[6], Lehti K[3,7], Salehi S[3,8], Puolakkainen P[1], Haglund C[1,9], Seppänen H[1], Leppä S[2,10,11]✉ and Ojala PM[1]✉.

[1]Translational Cancer Medicine Research Program, Faculty of Medicine, University of Helsinki, Helsinki, Finland. [2]Applied Tumor Genomics Research Program, Faculty of Medicine, University of Helsinki, Helsinki, Finland. [3]Department of Microbiology, Tumor and Cell Biology, Karolinska Institutet, Stockholm, Sweden. [4]Laboratory Animal Center, Helsinki Institute of Life Science-HiLIFE, University of Helsinki. [5] Department of Pathology, University of Helsinki and Helsinki University Hospital.[6]Department of Oncology-Pathology, Karolinska Institutet, Stockholm, Sweden. Keck School of Medicine, University of Southern California, Los Angeles, US. [7]Department of Biomedical Laboratory Science, Norwegian University of Science and Technology, Trondheim, Norway. [8]Department of Pelvic Cancer, Theme Cancer, Karolinska University Hospital, Stockholm, Sweden. [9]Department of Surgery, University of Helsinki and Helsinki University Hospital. [10]Department of Oncology, Helsinki University Hospital Comprehensive Cancer Center, Helsinki, Finland. [11]iCAN Digital Precision Cancer Medicine Flagship, 00014 Helsinki, Finland.

Running title: SSEA-4 CAR-T cells in solid tumors.

Keywords: SSEA-4, OVARIAN CANCER, CAR-T cells, efficacy, toxicity.

Additional information

✉Authors to whom correspondence should be addressed (paivi.ojala@helsinki.fi; sirpa.leppa@helsinki.fi).

[*]Equal contribution to this work as first authors.

[#]Equal contribution to this work as second authors.

Abstract

Chimeric antigen receptor (CAR) T-cell immunotherapies for solid tumors face critical challenges such as heterogeneous antigen expression. We characterized SSEA-4 cell-surface glycolipid as a target for CAR-T cell therapy. SSEA-4 is mainly expressed during embryogenesis but is also found in several cancer types making it an attractive tumor-associated antigen. Anti-SSEA-4 CAR-T cells were generated and assessed pre-clinically *in vitro* and *in vivo* for anti-tumor response and safety. SSEA-4 CAR-T cells effectively eliminated SSEA-4 positive cells in all tested cancer cell lines whereas SSEA-4 negative cells lines were not targeted. In vivo studies using NSG mice and the high-grade serous ovarian cancer cell line OVCAR4 demonstrated a remarkable and specific anti-tumor response at all CAR-T cell doses used. At high T cell doses, CAR-T cell-treated mice showed signs of health deterioration after a follow-up period. However, severity of toxicity was reduced with delayed onset when lower CAR-T cell doses were used. Our data demonstrate the efficacy of anti-SSEA-4 CAR-T therapy; however, safety strategies, such as dose-limiting and antibody-dependent cellular cytotoxicity, should be implemented for its potential clinical translation.

Introduction

Cancer immunotherapies aimed at harnessing the immune system to fight refractory malignancies are rapidly evolving and have a promising potential. Based on the cancer immunosurveillance hypothesis (Ochsenbein, 2002), chimeric antigen receptor T (CAR-T) cell therapies targeting CD19 (Greenbaum *et al*, 2020) have shown remarkable success in acute lymphoblastic and B-cell lymphomas (Waldman *et al*, 2020). In CAR-T cell therapy, patients' T cells are genetically engineered *ex vivo* to express synthetic single-chain variable fragment (scFv) chimeric antigen receptors (CAR) against tumor antigens and subsequently infused back into patients, mounting a cytotoxic anti-tumor response upon antigen recognition (Walsh *et al*, 2019).

In contrast to hematological malignancies, CAR-T cell therapies for solid tumors have produced limited efficacy and currently face multifactorial challenges for successful clinical translation. Solid tumors grow in functional association with the tumor microenvironment (TME) (Anderson & Simon, 2020). Typically composed of immune and stromal cells, blood vessels, and extracellular matrix (ECM), the TME constitutes a physical barrier and hostile immunosuppressive environment that CAR-T cells must overcome to target cancer cells (Rafiq *et al*, 2020; Rodriguez-Garcia *et al*, 2020). Furthermore, solid tumors are heterogeneous and express a diversity of tumor-associated antigens (TAA), which impair single-antigen CAR-T cell efficacy and lead to antigen escape and tumor relapse. Addressing these challenges in CAR-T cell therapy for solid tumors is thus necessary, and innovative strategies, such as the identification of actionable tumor antigens and cancer stem-like cell (CSC) targeting, are currently under active investigation (Newick *et al*, 2017; Wagner *et al*, 2020; Yamamoto *et al*, 2019).

CAR-T cells can trigger life-threatening toxicities, including cytokine release syndrome (CRS), neurotoxicity, and on-target off-tumor activity due to TAA expression in normal tissues (Sterner & Sterner, 2021). Management strategies for CAR-T cell therapy toxicities involve systemic immunosuppression, CAR-T cell depletion using antibody-dependent cytotoxicity (ADCC), and CAR-T cell dose evaluation to prevent potential off-targeting (Brandt *et al*, 2020; Brudno & Kochenderfer, 2016; Dasyam *et al*, 2020). Analogous to normal stem cells (SCs), CSCs are a rare and persistent subpopulation of cancer cells with a strong ability to self-renew and produce heterogeneous progenitor cells that comprise the bulk of the tumor. CSCs have been identified in various malignancies, including ovarian, pancreatic, and gastric cancers (Addeo *et al*, 2021; Askan *et al*, 2021; Terraneo *et al*, 2020), and are considered drivers of tumorigenesis, metastasis, and

84 cancer progression owing to their therapeutic resistance. Accordingly, CSCs constitute a potential
85 key target for CAR-T cell therapy (Alhabbab, 2020; Prager *et al*, 2019).
86
87 Stage-specific embryonic antigen-4 (SSEA-4) is a developmentally regulated glycosphingolipid
88 (GSL). SSEA-4 expression has been reported to be restricted mainly to early embryogenic stages
89 and pluripotent SCs and is mostly absent in differentiated cells and tissues (Russo *et al*, 2018).
90 GSLs play essential roles in cell adhesion, proliferation, and signal transduction. Consistently,
91 malignant transformation encompasses cellular GSL re-programming (Munkley & Elliott, 2016). In
92 functional association with tumorigenesis and cancer progression (Sivasubramaniyan *et al*, 2015),
93 SSEA-4 is expressed in ovarian, breast, lung, pancreatic, and brain cancer cells, as well as in breast
94 and ovarian CSCs (Ho *et al*, 2017; Parte *et al*, 2018), thereby making SSEA-4 an attractive target
95 antigen for CAR-T cell therapy (Firuzi *et al*, 2019; Lou *et al*, 2014a; Soliman *et al*, 2020). In this
96 study, we analyzed the expression of SSEA-4 in different human tumor tissues, as well as in
97 cultured ovarian, pancreatic, and gastric cancer cell lines, and tested SSEA-4-targeting CAR-T cells
98 pre-clinically *in vitro* and *in vivo* for their therapeutic efficacy and safety.
99
100 **Results**
101
102 **Characterization of SSEA-4 expression in human cancer specimens and cell lines.**
103 SSEA-4 expression has been demonstrated in various types of cancer (Sigal *et al*, 2022). To
104 corroborate and extend previous findings, we stained formalin-fixed paraffin-embedded (FFPE)
105 clinical gastric cancer samples. We observed only a low signal or complete absence of SSEA-4
106 immunoreactivity in all studied samples (Supplementary Fig. S1A). Next, we investigated whether
107 the lack of specific staining was due to the organic solvent treatment normally used during staining
108 of FFPE samples. In fresh frozen (FF) tumor samples, we detected strong SSEA-4
109 immunoreactivity in several cancer types, including gastric cancer (Fig. 1A-C). In contrast, the
110 treatment of FF tumor tissue sections with a standard xylene/ethanol series resulted in SSEA-4
111 signal loss (Supplementary Fig. S1B). This finding indicates that the organic solvent treatment is
112 not suitable for SSEA-4 detection. To confirm the specificity of the anti-SSEA-4 antibody, we
113 stained FF pancreatic cancer samples with soluble SSEA-4 hexaose (blocking glycan). This resulted
114 in the loss of the SSEA-4 signal, which was specific for SSEA-4, as the closely related glycolipid,
115 SSEA-3, did not block SSEA-4 immunoreactivity (Supplementary Fig. S1C). SSEA-4 expression
116 was heterogeneous in FF tissues from ovarian (OC), pancreatic (PC), and gastric (GC) cancers (Fig.
117 1A-C). In OC, 19 of 22 samples (86%) expressed SSEA-4 with variable intensity and extent (Fig.

118 1A). In some samples, SSEA-4 expression was observed in both tumor cells and the surrounding
119 stroma, whereas in others, its expression appeared to be restricted to the stroma. Focusing on OC,
120 and for a more precise analysis, we performed double immunofluorescence staining for SSEA-4 and
121 tumor cell-specific PAX8, which revealed the localization of SSEA-4 in tumor cells or stroma (Fig.
122 1A). In PC, 19 of 23 samples (83%) expressed SSEA-4 (Fig. 1B). Tumor cell and acinar cell
123 immunoreactivity were also detected. Similar to OC cases, some samples showed SSEA-4 signals
124 only in the stroma. In GC, eight of the nine samples (89%) were positive for SSEA-4, with
125 expression mostly localized to tumor cells (Fig. 1C).
126
127 To find suitable SSEA-4 expressing cell models, we analyzed SSEA-4 expression in a variety of
128 cancer cell lines using FACS. Some cell lines representing the aforementioned cancer types were
129 either highly positive (OVCAR4, HPAC, and MKN45; OC, PC, and GC, respectively) or very
130 low/negative (Caov-3, MIA PaCa-2, and MKN28; OC, PC, and GC, respectively) for SSEA-4 (Fig.
131 1D). The FACS results were further confirmed by immunofluorescence staining of OC cell lines
132 (Supplementary Fig. S1D).
133
134 **Generation and *in vitro* characterization of SSEA-4 specific CAR-T cells.**
135 To obtain optimal expression of a long RNA encoding multiple gene products and to fulfil
136 regulatory requirements in future clinical trials, a previously described anti-SSEA-4 CAR vector
137 (Lin *et al*, 2021) was modified by replacing the cytomegalovirus (CMV) promoter with EF-1α
138 (human elongation factor-1 alpha) and ampicillin (AmpR) cassette with kanamycin (KanR). For cell
139 selection, tracking, and CAR-T cell depletion by cetuximab-mediated ADCC, a truncated human
140 epidermal growth factor receptor (EGFRt) (Wang *et al*, 2011) (Fig. 2A) was inserted downstream of
141 the CD28 and CD3zeta sequences (costimulatory/activation domains). A poly A-like sequence in
142 EGFRt was also removed. Anti-SSEA-4 CAR-T cells (hereinafter referred to as CAR-T) were
143 generated from healthy donor-derived $CD4^+$ and $CD8^+$ T cell populations, transduced at efficiencies
144 ranging from to 35-90% (Fig. 2B and C), and expanded for 10-12 days with $CD4^+/CD8^+$ ratios of ≈
145 1 (Fig. 2D and E). Non-transduced T-cells from the same donor (NT-T) were used as control.
146
147 To assess CAR-T anti-tumor response and specificity, we performed *in vitro* cytotoxicity assays in
148 SSEA-4^+ OVCAR4 (OC), HPAC (PC), and MKN45 (GC), as well as in SSEA-4^- Caov-3 (OC),
149 MIA PaCa-2 (PC), and MKN28 (GC) human cell lines. The specificity and efficacy of CAR-T cells
150 were evaluated at different T-cell doses in comparison with NT-T and GFP (mock) CAR-T cells.
151 CAR-T cells killed SSEA-4^+ OC, PC, and GC cells efficiently (Fig. 2F) but did not show any

152 significant cytotoxic activity against SSEA-4$^-$ cells. NT-T and GFP CAR-T cells showed no effect
153 on any cell type tested, further corroborating the specific SSEA-4 targeted anti-tumor response of
154 the CAR-T cells. The CAR-T cell response was dose-dependent and detectable at E:Ts (effector :
155 target cell ratios) as low as 0.12 in all SSEA-4$^+$ cell lines tested. In contrast to NT-T cells, the
156 interaction of CAR-T cells with OVCAR4 cells, but not with Caov-3 cells, induced T-cell
157 proliferation (Fig. 3A-C), indicating T-cell activation in response to SSEA-4. A significant increase
158 in IFNγ and IL2 secretion was also observed in CAR-T cells, but not in NT-T cells, when co-
159 cultured with OVCAR4 cells (Fig. 3D and E), further supporting the specific SSEA-4 -induced
160 functional activation of CAR-T cells. To evaluate a potential safety strategy, we assayed ADCC *in*
161 *vitro* using a cetuximab antibody targeting EGFRt (Brandt *et al.*, 2020). CAR-T cells were
162 efficiently depleted by NK cells in response to two different concentrations of cetuximab, but not
163 when NK + CAR-T cells were co-cultured without cetuximab (Fig. 3F).
164
165 **SSEA-4 CAR-T cells produce robust anti-tumor response in the OVCAR4 xenograft model.**
166 Next, we evaluated the *in vivo* efficacy of SSEA-4 CAR-T cells in ovarian cancer cell xenografts.
167 NSG (NOD scid gamma) female mice were implanted intraperitoneally (i. p.) with 2x10^6 luciferase-
168 and GFP-expressing OVCAR4 cells. After 13 days, mice were infused intravenously with T cell
169 doses of 1x10^6, 2x10^6 and 3x10^6 CAR-T cells (hereinafter referred as 1M, 2M and 3M),
170 corresponding to 2.9x10^6, 5.7x10^6 and 8.6x10^6 of total T cells based on 35% lentivirus transduction
171 efficiency in the cell batch used in this experiment. Control mouse groups were infused with PBS or
172 an NT-T cell dose equal to the total T cell number in the CAR-T groups (Supplementary Fig. S2A).
173 Thirty-two days after T-cell infusion, CAR-T cell-treated mice in all dose groups presented a
174 remarkable and specific reduction in tumor burden, in contrast to PBS- and NT-T cell-treated mice
175 showing continuous tumor growth (Fig. 4A-D). However, mice treated with the 3M dose of NT-T
176 cells displayed a similar reduction in tumor burden as the CAR-T cell-treated group, revealing an
177 upper threshold of ≈ 5-6x10^6 total T cells for the specific anti-tumor response in the OVCAR4 i. p.
178 xenograft model (Fig. 4D). All mice remained in apparently good body scoring conditions (BCS ≈
179 3) during the 32-day experiment, except for 3M CAR-T mice, which showed a trend for weight loss
180 at the later stages. (Supplementary Fig. S2B). T cell activation was confirmed by measuring IFNγ
181 levels in post-mortem mouse blood samples. IFNγ secretion was significantly elevated in mice
182 treated with 1M, 2M and 3M CAR-T cell doses compared to mice infused with PBS or NT-T cells.
183 In line with the anti-tumor response of NT-T cells at high doses, elevated levels of IFNγ were also
184 detected in 3M NT-T cell-treated mice (Supplementary Fig. S3A). Bioluminescence imaging (BLI)

185 of the post-mortem organs corroborated the specific reduction in tumor burden in mice treated with
186 1M, 2M and 3M CAR-T doses, showing a substantially reduced signal in all organs examined when
187 compared to PBS- and NT-T-treated mice. The cancer cell signal in our OVCAR4 xenograft model
188 was preferentially associated with the spleen, pancreas, ovaries, intestine, and stomach. Similar to
189 the whole-body BLI results, mice treated with the 3M NT-T cell dose showed reduced organ BLI
190 signal (Supplementary Fig. S3B and C). In contrast to OVCAR4-engrafted CAR-T mice, human
191 gene expression, including *ACTB*, *TIM-3*, *LAG-3*, and *PD-1*, was detected at very low levels in
192 post-mortem blood samples of OVCAR4-engrafted PBS-treated control mice (Supplementary Fig.
193 S4A-C), thereby indicating that the detection of human gene expression in OVCAR4-engrafted
194 CAR-T mice originated mostly from human T cells, and further allowed for an approximate
195 analysis of the CAR-T exhaustion phenotype in mice. As shown in (Supplementary Fig. S4D-F),
196 the expression of *TIM-3*, *LAG-3* and *PD-1* T cell exhaustion markers in CAR-T mice was dose-
197 dependent and significantly elevated at 3M doses compared to 1M and 2M doses. Altogether, the
198 data indicated that at lower doses (1M and 2M), anti-SSEA-4 CAR-T cells were highly effective,
199 with a robust and specific anti-tumor response and reduced exhaustion phenotype in the OVCAR4
200 xenograft models.
201
202 **SSEA-4 CAR-T cells cause long-term adverse effects.**
203 Although there was no apparent toxicity in mice in the above-described 32-day efficacy *in vivo*
204 study, modest signs of toxicity were observed in mice treated with the 3M CAR-T cell dose. We
205 therefore carried out a long-term (70-day), safety, efficacy, and survival assay *in vivo* using 1M and
206 2M CAR-T cell doses, corresponding to $1.1x10^6$ and $2.2x10^6$ T cells based on 90% lentivirus
207 transduction in the cell batch used in this experiment (Supplementary Fig. S5A). As previously
208 described, tumor-bearing control mice were infused with PBS or an NT-T cell dose corresponding
209 to the total number of T cells in the CAR-T groups. Tumor-free mice treated with a 1M dose were
210 used to assess the potential toxicity of CAR/NT-T cells in the absence of OVCAR4 cells.
211
212 Corroborating the anti-tumor response of SSEA-4 CAR-T cells, both CAR-T doses led to a
213 reduction in tumor burden compared to PBS treatment. While the 1M dose NT-T mice showed no
214 significant reduction in their tumor burden, the NT-T 2M dose produced a significant anti-tumor
215 response at the later stages of the 70-day treatment (Fig. 4E and F, Supplementary Fig. S5B and C).
216 Consistent with the anti-tumor activity of CAR-T cells, mice treated with both 1M and 2M doses
217 showed elevated levels of IFNγ and TNFα (Fig. 4G and H). All mice remained in good health
218 during the first 35-40 days of treatment. However, thereafter, some tumor-bearing CAR-T cell-

219 treated mice showed weight loss, inactivity, and an overall low BCS (≈ 1-2). Three out of 10 mice
220 with 1M dose, and 5 out of 10 mice with 2M dose, had to be sacrificed before the experimental
221 endpoint (Supplementary Fig. S5 and S6), translating in 70% and 50% survival rates, respectively
222 (Fig. 4I). PBS, and the remaining CAR-T and NT-T mice were active and showed a good overall
223 condition (BCS ≈ 3) and normal activity without signs of health deterioration. Similarly, tumor-free
224 mice treated with CAR-T and NT-T cells remained healthy and active during the 70-day study
225 period (Supplementary Fig. S6). Altogether, our data demonstrated the specific anti-tumor response
226 of SSEA-4 CAR-T cells, even at relatively low doses. At high doses, CAR-T cells produced
227 apparent toxicities in mice, thus precluding clinical translation at this stage.
228
229 **SSEA-4 targeting of normal mouse cells as a potential cause for the *in vivo* adverse events**
230 **during long-term SSEA-4 CAR-T cell treatment.**
231 To examine the possible on-target off-tumor effects in mice treated long-term with SSEA-4 CAR-T
232 cells, we analyzed the expression of SSEA-4 in normal mouse tissues. Prominent SSEA-4
233 expression was detected in the kidneys, stomach, and intestine and, to a lesser extent, in the brain
234 and heart. The SSEA-4 signal was sparse in the lungs, whereas the spleen, pancreas, and liver were
235 mostly devoid of SSEA-4 (Supplementary Fig. S7).
236
237 Histopathological analysis of post-mortem tissues was performed on tissues with high (kidney and
238 intestine) or moderate (lung) SSEA-4 expression. The analysis included the estimation of
239 lymphocyte infiltration and tissue damage, each graded on a scale from 0 to 3. Analysis of the
240 H&E-stained sections revealed perivascular/peribronchiolar lymphocyte infiltrates in the lungs, and
241 in the intestinal wall of the CAR-T-treated mice compared to the NT-T-treated mice (average
242 grading 0 *vs* 1.43, respectively for mice treated with 2M doses; Supplementary Fig. S8A). Signs of
243 aspiration pneumonia were observed in three CAR-T cell-treated and prematurely euthanized mice.
244 However, there was no apparent, histologically appreciable, direct damage to the parenchymal cells
245 (Supplementary Fig. S8A).
246
247 To further corroborate the histopathological findings, we performed IF staining of T cells (CD3)
248 and CAR-T cells (anti-EGFR) in the lungs, kidneys, and intestine (Supplementary Fig. S8B).
249 Consistent with H&E staining, the most prominent T cell deposits were observed in the lungs of
250 both CAR- and NT-T cell-treated mice. CAR-T cells were also detected in the intestinal wall of
251 CAR-T cell-treated mice. NT-T cells were not observed in NT-T-treated mice in the tissues
252 analyzed.

253
254
255
256 **Discussion**
257
258 CAR-T cell therapy approaches in solid tumors face multifactorial challenges, including
259 identification of actionable tumor antigens (Sterner & Sterner, 2021). To tackle this obstacle, we
260 conducted a pre-clinical CAR-T cell study using SSEA-4 as a TAA in an ovarian cancer model.
261
262 SSEA-4 has been shown to be expressed in pluripotent SCs, and developmentally regulated (Russo
263 *et al.*, 2018). Consistent with its role in proliferation and migration, aberrant expression of SSEA-4
264 confers tumor cells with malignant stem-like traits such as proliferation, drug resistance, and
265 metastasis (Magalhães *et al*, 2017; Munkley & Elliott, 2016). Thus, SSEA-4 reprogramming of
266 tumor cells provides an attractive target for CAR-T therapies in solid tumors. In line with this,
267 CAR-T cells targeting glycans such as MUC1 and GD2 have shown high therapeutic potential
268 against triple-negative breast cancer and glioblastoma (Prapa *et al*, 2021; Zhou *et al*, 2019).
269 Moreover, SSEA-4 CAR-T cells enable targeting of tumor cells with potential stem-like properties
270 (CSCs), which are closely associated with tumor heterogeneity and relapse (Ho *et al.*, 2017; Lou *et*
271 *al*, 2014b; Prager *et al.*, 2019). Clinical trials using CAR-T cells against CSC markers include
272 CD133, CD171, and c-Met for ovarian, brain, and breast cancers and neuroblastoma (Masoumi *et*
273 *al*, 2021).
274
275 Confirming previous results (Sigal *et al.*, 2022), SSEA-4 expression was detected in most of the
276 cases of ovarian, pancreatic, and gastric cancer tissues. Based on the positive SSEA-4 expression in
277 several cancer types, anti-SSEA-4 CAR-T cells were generated and functionally characterized for
278 specific and effective anti-tumor response and safety.
279
280 SSEA-4 CAR-T cells showed specific and effective anti-tumor responses *in vitro* in SSEA-4^+
281 ovarian, pancreatic, and gastric tumor cell lines. CAR-T cells produced elevated levels of IFNγ and
282 IL-2 in killing assays with ovarian cancer cells and, corroborating the specific interaction with
283 SSEA-4, CAR-T cell proliferation was induced in co-cultures with SSEA-4^+ ovarian cancer cells.
284 Current strategies to overcome CAR-T cell therapy challenges involve engineering CAR-T cells
285 with powerful anti-tumor activity (Sterner & Sterner, 2021). In this respect, SSEA-4 CAR-T cells
286 demonstrated effective SSEA4^+ targeting, even at very low E:T ratios in all *in vitro* cancer models.

287

288 High-grade serous ovarian carcinomas (HGSOC), represented by OVCAR4 cells in this study,
289 constitute the most common and lethal gynecologic malignancies, typically forming
290 immunologically "cold" tumors that are unresponsive to immune checkpoint blockage (Wu *et al*,
291 2021). To date, responses to CAR-T therapies in HGSOCs have been relatively poor, mainly due to
292 the deficient anti-tumor response of T cells and poor infiltration capacity in the tumor tissue
293 (Wagner *et al.*, 2020). In our *in vivo* OVCAR4 xenograft models, SSEA-4 CAR-T cells produced
294 an effective anti-tumor response at dose levels ranging from 1M to 3M, thereby indicating that they
295 could infiltrate into the tumor tissue and develop potent anti-tumor activity.

296

297 In a long-term safety assessment, SSEA-4 CAR-T cells produced severe adverse events in some
298 mice, manifested by abnormal inactivity and progressive weight loss, indicating a dose-limiting
299 toxicity for SSEA-4 CAR-T cells. Notably, in our OVCAR4 xenograft model, lower CAR-T cell
300 doses produced an effective anti-tumor response, which was similar to that observed at higher
301 CAR-T cell doses, but with a delayed onset and reduced severity of adverse effects. Moreover, 1M
302 dose CAR-T cell-treated mice with moderate weight loss at the early stages of the treatment
303 progressively regained weight to normal levels and remained active and in good health condition
304 (BCS ≈ 3) until the end of the study. The severity of the CAR-T cell associated adverse events is
305 related, among the others, to CAR-T cell potency and dose (Zhou *et al*, 2020). Increasing the
306 number of CAR-T cells has been shown to enhance tumor clearance but may also increase the risk
307 of toxicities (Mehta *et al*, 2021). In line with this, strategies to prevent and manage toxicities
308 include treatment with low or split doses of CAR-T cells (Green *et al*, 2018; Jiang *et al*, 2018).
309 Based on our results, it is conceivable that, at very low doses or with a lower affinity scFv, SSEA-4
310 CAR-T cells could exert a potent anti-tumor response with minimal toxicity.

311

312 Targeting CSCs with CAR-T cell therapy constitutes a promising strategy for tumor eradication
313 (Cui *et al*, 2021; Masoumi *et al.*, 2021). However, the expression of CSC antigens may also occur
314 in normal stem cells, thus increasing the risk of on-target off-tumor toxicities. In this regard,
315 infiltrated SSEA-4 CAR-T cells in the SSEA-4 positive mouse intestinal wall may have impaired
316 the normal absorption function of the gut, even though no direct damage to the epithelium was
317 detected. Similarly, prominent lymphocyte infiltration was observed in the lungs of the CAR-T cell-
318 treated mice. Accumulation of SSEA-4 CAR-T cells in the lungs and intestine might have produced
319 severe inflammation, thereby affecting the normal respiratory and digestive functions in CAR-T-
320 treated mice.

Tumor-free mice treated with CAR/NT-T cells at 1M dose showed no signs of health deterioration and remained active and healthy throughout the study. The absence of toxicities in these mice, and in contrast to tumor-bearing mice, strongly suggests that an OVCAR4-dependent over-stimulated SSEA-4 CAR-T cell immune response caused serious adverse effects. NT-T cells at 3M dose, and to some extent at 2M dose, also reduced OVCAR4 tumor burden, thereby demonstrating a CAR-independent anti-OVCAR4 response. Further supporting this notion, our *in vitro* results showed a dose-dependent anti-OVCAR4 response in NT-T cells. Moreover, a recent study using SSEA-4 CAR-T cells in a pancreatic NSG mouse xenograft model showed no anti-tumor response for NT-T cells at doses up to 5M (Lin *et al.*, 2021). Taken together, these data indicate that OVCAR4 cells may be particularly prone to elicit CAR-independent, high tumor-specific T cell reactivity (Disis *et al*, 2009). Accordingly, at high CAR-T cell doses, the occurrence of both CAR-dependent and CAR-independent interactions with OVCAR4 tumor tissues could have resulted in over-stimulated T-cell activation, proliferation, inflammation, and damage to SSEA-4 positive normal tissues.

In conclusion, this study demonstrated the efficacy of SSEA-4 CAR-T cells in an HGSOC pre-clinical model. However, SSEA-4 CAR-T cell therapy produced severe adverse effects; therefore, further assessment and/or toxicity management strategies are required for its clinical translation. Alternative strategies could involve lowering the CAR-T cell dose or scFv affinity, ADCC, equipping CAR-T cells with combinatorial antigen recognition (Choe *et al*, 2021; Kloss *et al*, 2013) such as SSEA-4 and mesothelin (Schoutrop *et al*, 2021), and/or sigmoidal antigen-density threshold (Hernandez-Lopez Rogelio *et al*, 2021) using low-affinity synthetic Notch receptors to control the expression of the high-affinity anti-SSEA-4 CAR.

Materials and methods

Tissue processing and staining. Fresh frozen HGSC tumor samples were embedded in Tissue-Tek OCT compound (Sakura Finetek), frozen, and cut into 8-µm cryosections. Frozen sections were placed in 4% PFA in PBS for 10 min and washed with PBS for 10 min. For immunofluorescence staining sections were blocked with TNB blocking buffer (0.1 M Tris–HCl, pH 7.5; 0.15 M NaCl; 0.5% (w/v) blocking reagent (PerkinElmer, Cat # FP1020) for 30 min at RT. The sections were incubated overnight at 4 °C in a humidified chamber with SSEA4 antibody (1:100, GTX48037, Genetex; SSEA-4 hexaose [Elicity #GLY131-90%] blocking glycan was used as a negative control at 100 µM). After washes with TNT (0.1 M Tris-Cl, pH 7.5; 0.15 M NaCl; 0.1% (v/v) Tween 20),

355 sections were incubated with PAX8 antibody (1:250, #10336-1-AP, Proteintech) and anti-mouse
356 Alexa Fluor Plus 555 secondary antibody in TNB for 90 min and washed with TNT. The sections
357 were then incubated with anti-rabbit Alexa Fluor Plus 488 secondary antibody in TNB for 90
358 minutes, washed with TNT, and rinsed with PBS. Slides were mounted with VECTASHIELD
359 Antifade Mounting Medium containing DAPI. Confocal micrographs of immunofluorescence
360 staining were obtained using a confocal microscope (LSM 800) with a C-Apochromat 40×, 1.2 NA
361 water objective lens, and a Plan-Apochromat 20×, 0.8 NA objective lens (Carl Zeiss). For
362 immunohistochemistry, sections were blocked with 3% BSA in PBS for 30 min and incubated with
363 SSEA-4 antibody (GTX48037, Genetex) overnight, followed by incubation with Brightvision poly
364 HRP-anti-mouse antibody, washing, DAB solution, and hematoxylin staining using standard
365 protocols.
366
367 **Cancer cell culture.** OVCAR4 and Caov3 (human ovarian adenocarcinoma; RRID:CVCL_1627
368 and LGC Nordic ATCC HTB-75, respectively), HPAC and MIA PaCa-2 (human pancreatic
369 adenocarcinoma; LGC Nordic, ATCC CRL-2119, and CRL-1420, respectively), and MKN45 and
370 MKN28 (human gastric adenocarcinoma; RRID:CVCL_0434 and RRID:CVCL_1416,
371 respectively) were cultured in RPMI medium (Roswell Park Memorial Institute 1640. #BE12-167F,
372 Gibco) supplemented with 10% fetal bovine serum (FBS, qualified Brazil. #10270106 Gibco), 2
373 mM L-glutamine (#BE17-605E, Gibco), 100 U/mL penicillin, and 100 µg/mL streptomycin
374 (#DE17-602E, Gibco) and subcultured in phosphate-buffered saline (1X; PBS. #MT21040CV,
375 Gibco) and trypsin-EDTA solution (#BE17-161E; Lonza, Basel, Switzerland). HEK293T cells
376 (human embryonic kidney; LGC Nordic ATCC CRL-3216) were cultured in DMEM high glucose
377 (#BE12-614Q, Lonza), supplemented with 2 mM L-glutamine, 10% FBS, 100 U/mL penicillin, and
378 100 µg/mL streptomycin, and sub-cultured with PBS and trypsin. All the cell lines were
379 authenticated using the Genome Analysis Infrastructure (HiLIFE; Helsinki Institute of Life Science)
380 and assayed at low passage numbers. All cells were incubated at 37°C in 5% CO2 and routinely
381 tested for mycoplasma-free status (Eurofins Genomic Europe, Germany).
382
383 **Flow cytometry analysis.** 0.5-1x10^6 Cells were labeled per tube in staining buffer (1% BSA/2 mM
384 EDTA/PBS). Cells were fixed with 4% PFA for 10 min (where appropriate) at room temperature,
385 3x washed in buffer (2 mM EDTA/PBS), blocked for 30 min in staining buffer, and subsequently
386 stained with primary and secondary antibodies in 100 µL volume, with 3x washes in between where
387 appropriate, and after staining. The cells were resuspended in 200 µL wash buffer and analyzed
388 using BD Accuri C6 Flow Cytometer Analyzer and Accuri Cflow Plus software. The gating

389 strategy followed FSC-A *vs* SSC-A size and granularity, FSC-H *vs* FSC-A doublets, and
390 corresponding FL *vs* FSC-A marker detection. Negative controls included isotypes, not stained
391 samples, and where appropriate NT-T cells were used. The following antibodies were used in this
392 study: Alexa Fluor 488 anti-human SSEA-4 (#330412, clone MC-813-70, Mouse IgG3 κ, dilution
393 1:100, Biolegend); Alexa Fluor 647 anti-human SSEA-4 Antibody (#330408, clone MC-813-70,
394 Mouse IgG3 κ, dilution 1:100, Biolegend); Cetuximab (#A2000, Human IgG1, dilution 1:100,
395 Selleckchem); Alexa fluor 488 Goat anti-Human IgG Secondary (#A-11013, dilution 1:100,
396 Invitrogen); APC anti-human CD4 Antibody (#357408, Rat IgG2b κ, dilution 1:20, Biolegend);
397 FITC anti-human CD8 Antibody (#344704, Mouse IgG1 κ, dilution 1:20, Biolegend); Alexa Fluor
398 647 anti-human CD3 Antibody (#300322, Mouse IgG2a κ, dilution 1:100, Biolegend); APC Rat
399 IgG2a κ Isotype Ctrl (#400512, dilution 1:20, Biolegend); FITC Mouse IgG κ Isotype Ctrl (#00108,
400 dilution 1:20, Biolegend); APC Mouse IgG2a κ Isotype Ctrl (#981906, dilution 1:100, Biolegend).
401
402 **Immunofluorescence.** OVCAR4 and Caov-3 cells were grown on glass coverslips at low
403 confluence for 24 h. Next, the cells were fixed with 4% PFA (#HL96753.1000, without methanol,
404 Histolab), blocked with staining buffer for 30 min, stained with Alexa Fluor 647 anti-human SSEA-
405 4 antibody (dilution 1:100) overnight at 4ºC, 3x washed with PBS, and counterstained with Hoechst
406 33342 (#H21492, Invitrogen). The slides were mounted with mowiol (#81381; Sigma-Aldrich).
407 Slides were visualized with Axio Imager (Zeiss upright epifluorescence microscope) with an EC
408 Plan Neofluar 40x 1.3 NA water objective lens and Plan-Apochromat 63x 1.4 NA oil objective lens
409 (Zeiss). Images were acquired using Hamamatsu Orca Flash 4.0 LT B&W camera for fluorescence
410 and Zeiss Zen 2 software.
411
412 **Luciferase/GFP expression.** Mammalian gene expression lentiviral vector pLV-
413 EF1A>Luc2:T2A:Puro:F2A:TurboGFP (#VB210127-1246ann, VectorBuilder) was used to produce
414 luc2/tGFP carrying lentivirus. The expression vector and packaging plasmids, pLP1, pLP2, and
415 pLP/VSVG, were transfected into HEK293T cells. The viral supernatant was collected after 72 h,
416 0.45µm filtered, and precipitated with PEG-it (#LV825A-1, System Biosciences). The virus
417 precipitates were resuspended in PBS and stored at -80°C. Tumor cells were transduced with a MOI
418 of 10 for 24 h using Vectofusin-1 (10 µg/mL; #130-111-163, Miltenyi Biotec), with the following
419 selection in Puromycin 1-2 µg/ml (#P8833, Sigma-Aldrich).
420
421 **Generation of anti-SSEA-4 and anti-GFP CAR vector.** The anti-SSEA-4 scFv was designed by
422 CHO Pharma USA Inc. and inserted into a 2nd generation CAR lentivector containing the CD28z

423 co-stimulatory/activation domains; EGFRt sequence was cloned downstream of the CD28z
424 sequence (Creative Biolabs; US). For anti-GFP CAR-T cells, anti-SSEA-4 scFv was replaced with
425 anti-GFP scFv (Creative Biolabs). The CMV promoter was replaced with EF-1α for optimal
426 expression of long RNA encoding multiple gene products, and the AmpR cassette was replaced
427 with KanR to fulfil regulatory requirements in pre-clinical assessment and clinical trials (FIMEA;
428 Finnish Medicines Agency) (Oxford Genetics; UK). VIVE Biotech (ES) identified and removed a
429 poly A-like sequence in EGFRt.
430
431 **Generation of human anti-SSEA-4 CAR-T cells.** Human blood samples (~ 40 ml) were obtained
432 from healthy donors at the Finnish Red Cross Blood Services (FRCBS) and subsequently diluted
433 1:4 in PBS. Peripheral blood mononuclear cells (PBMCs) were separated by density gradient
434 centrifugation using Ficoll-Paque Premium (#17-5442-02; GE Healthcare). PBMCs were washed
435 3x with PBS, filtered with a 30 µm cell strainer (#43-50030-03, Pluriselect), and cryopreserved in
436 cryotubes (#177280, Nunc) in LN2 at $20x10^6$ cells/ml in 10% DMSO (cell culture reagent,
437 #02196055-CF, MPBio)-Albunorm (200 g/l, #054343, Octopharma). CAR-T cells were generated
438 following the Miltenyi protocol using TexMACS medium (#130-097-196), human CD4+ and CD8+
439 T-cell isolation kits (#130-096-533 and #130-096-495, respectively), T Cell TransAct human
440 (#130-111-160), human IL-7/IL-15 cytokines (#130-095-362 and #130-095-764, respectively), and
441 Vectofusin-1 (#130-111-163, Miltenyi Biotec). Briefly, PBMCs were thawed in a 37°C water bath
442 for a few minutes, washed 2x with TexMACS medium, and incubated in TexMACS for 3 h.
443 Subsequently, $CD4^+$ and $CD8^+$ T cells were isolated, combined, and activated/expanded in
444 TexMACS medium supplemented with TransAct, IL7 (500 IU/mL), and IL-15 (84 IU/mL). After
445 24 h, CD4+ and CD8+ T cells were transduced with anti-SSEA-4 CAR lentivirus with a MOI of 5
446 for 24 h, using Vectofusin-1 (10 µg/mL) and spinoculation (800 × g for 30 min at 32°C).
447 Subsequently, the culture medium was replaced with TexMACS supplemented with cytokines, and
448 the cells were cultured for an additional 8-10 days, with half of the media changed every 2-3 days.
449 For anti-GFP (mock) CAR-T cells, CD4+ and CD8+ T cells were transduced with anti-GFP CAR
450 lentivirus.
451
452 **Cytotoxicity assays.** Cytotoxic killing of target cells was assessed using Thermo Scientific Black
453 96-Well Immuno Plates. Tumor cells were plated at $0.5x10^4$ (OVCAR4) and $1x10^4$ (Caov-3,
454 HPAC, MIA Paca-2, MKN45, and MKN28) cells/well. All target cells expressed the Firefly
455 luciferase (FLuc) and turboGFP (tGFP) reporter genes to facilitate detection. After overnight
456 culture, anti-SSEA4, anti-GFP CAR-T, and NT-T cells were added at the indicated E:T (effector :

457 target cell ratio), and incubated for 72 h. Cell viability was measured using the Steady-Glo
458 Luciferase Assay System (Promega) as indicated by the manufacturer in FLUOstar Omega Filter-
459 based multi-mode microplate reader (BMG LabTech). Tumor cell-killing efficacy is represented as
460 % cell viability relative to untreated cultures (E:T=0).
461
462 **CFSE-dilution assay T cell proliferation.** CAR and NT-T cells were labeled with CFSE
463 (#C34554, CellTrace CFSE Cell Proliferation Kit Molecular Probes) according to the
464 manufacturer's instructions and at 1μM working concentration. $2.5x10^5$ CAR or NT-T cells were
465 incubated with SSEA-4 and SSEA-3 (#GLY131 and #GLY122, respectively, Elicityl-Oligotech) at
466 200 μM for 48 h in 24 well plate (Nunc). $5x10^5$ CAR and NT-T cells CFSE-labeled were incubated
467 with or without $1x10^6$ OVCAR4 and Caov-3 cells for 48 h in RPMI-10% FBS-Pen/Strep and L-
468 Glut medium in 10 cm cell culture dishes (Nunc). CFSE dilution was analyzed using flow
469 cytometry on $CD3^+$-gated cells; isotype/unstained cultures were used as $CD3^-$ control gating, and
470 CFSE-unlabeled CAR and NT-T cells were used as gates for negative CFSE detection. Cell
471 proliferation was assessed in relation to the corresponding CFSE-labeled CAR and NT-T cells
472 cultured in the absence of cancer cells.
473
474 **Cetuximab-based antibody-dependent cellular cytotoxicity.** Human NK cells were isolated from
475 PBMCs using the NK Cell Isolation Kit, human (#130-092-657, Miltenyi), according to the
476 manufacturer's instructions, and subcultured for 72 h in NK MACS medium supplemented with 5%
477 human serum male AB plasma (#H4522, Sigma-Aldrich) and human IL-2 IS (200 IU/ml, # 130-
478 097-746). Next, $0.5x10^6$ NK cells were incubated with $1x10^6$ CAR-T cells in the presence of 5-10
479 μg/ml human cetuximab. After 72 h, the cultures were washed and stained sequentially with CD3
480 and 1 μg recombinant protein L PE-conjugate (#11044-H07E-P, SinoBiological) following the
481 manufacturer's recommendations. CAR-T cell viability was assessed using flow cytometry on
482 $CD3^+$-gated T cells, and isotype/unstained cultures were used for $CD3^-$ control gating.
483
484 **Cytokine secretion in *in vitro* assays.** Secretion of human IFNγ was assessed from the supernatants
485 of cytotoxic assays where cancer and T cells were co-cultured for 72 h in a 24-well format ($0.5x10^5$
486 CAR and NT-T cells co-cultured with $1x10^5$ OVCAR4 cells), and mouse plasma samples, using
487 ELISA MAX Deluxe Set human (IFNγ #430104, IL-2 # 431804, and IL-6 #430504, BioLegend)
488 according to the manufacturer's instructions. The absorbance was measured at 450 nm using
489 FLUOstar reader.

490

491 **Animals and ethics statement.** All mice were housed in the Laboratory Animal Center facility,
492 Biomedicum 1, Helsinki University, under pathogen-free conditions and in ambient rooms with a
493 12 h light/dark cycle, filtered air at 22 ± 2°C temperature, and 55 ± 15% relative humidity. Mice
494 were caged in groups of two or three per IVC cage (Green-Line mice. Emerald. Tecniplast) on
495 autoclaved ASPEN wood chip bedding, with ad libitum access to laboratory chow (Tekland Global
496 Rodent Diet; T2916CMI.16) and sterile water. Animal experiments in this study were approved by
497 the Finnish National Animal Experiment Board (Eläinkoelautakunta ELLA. Approved license:
498 ESAVI/10548/2019) and conducted in accordance with the Finnish Act on the Protection of
499 Animals Used for Scientific or Educational Purposes, and the University of Helsinki guidelines.

500

501 **Animal studies and bioluminescence imaging.** Female NSG NOD.Cg-Prkdc^{scid} Il2rg^{tm1Wjl}/SzJ
502 mice (4–5 weeks old) were purchased from The Jackson Laboratory (Scanbur). 2x10^{6} OVCAR4
503 Fluc-tGFP cells, in 100 µL PBS, were injected intraperitoneally into isoflurane-anesthetized mice
504 (Attane vet, 100 mg/g) and grown for 13 days. Subsequently, CAR and NT-T cells were infused
505 intravenously (d0) at the specified T-cell dose in 100 µl PBS. *In vivo* CAR-T cell dose is defined in
506 this study as the specific number of CAR-T cells and was calculated based on the transduction
507 percentage. Equal numbers of NT-T cells were used for each cell dose (Supplementary Fig. S2 and
508 S5). For the no-treatment control group, mice were infused with 100 µL of PBS. Tumor progression
509 was monitored by BLI with CoA D-luciferin sodium salt substrate (#bc218, Synchem) injected
510 intraperitoneally at 150 mg/kg. Bioluminescence images were acquired 10 min after D-luciferin
511 injection with the SPECTRAL Lago X Imaging System and analyzed with Aura Imaging Software
512 v3.1.0 (Spectral Instruments Imaging). Mice were monitored at regular intervals for behavior,
513 activity, feeding, and weight. At the end of the experiment, the mice were anesthetized with
514 ketamine-xylazine (#511485, Intervet; #148999, Orion Pharma) and blood samples were collected
515 via cardiac puncture in EDTA capillary tubes (#076012, Kabe Labortechnik). Plasma and blood
516 cells were separated by centrifugation (500 × g for 5 min at 4°C) and stored at -80°C.
517 Organs/tissues were collected post-mortem, imaged for bioluminescence, and fixed/stored in 4%
518 PFA (without methanol) at 4°C.

519

520 **Cytokine secretion in *in vivo* assays**. Human cytokine secretion was assessed in mouse plasma
521 samples using the Human XL Cytokine Luminex Performance Panel Premixed Kit (#FCSTM18,
522 R&D Systems), according to the manufacturer's instructions.

523

524 **RNA isolation and qPCR.** Mouse blood cells were pelleted by centrifugation, washed with 1x PBS
525 at 4°C, resuspended in Trisure (#BIO-38032, Bioline), and homogenized with high-density
526 zirconium oxide beads in a PowerLyzer (Mo Bio). Chloroform was added, mixed, and the samples
527 were centrifuged at 11000 × g for 10 min at 4ºC °C. The upper aqueous phase was subsequently
528 used for RNA isolation using the NucleoSpin RNA, Mini it for RNA purification (#740955.50,
529 Macherey-Nagel), and cDNA was synthesized using iScript Reverse Transcription Supermix
530 (#1708841, Bio-Rad). Gene expression was assessed using TaqMan assays (Thermo Fisher), human
531 ACTB (Hs99999903_m1), human LAG-3 (#Hs99999160_m1), human TIM-3/HAVCR2
532 (#Hs00958618_m1), human PD-1/PDCD1 (#Hs1550088_m1), and mouse Gapdh
533 (Mm03302249_g1), according to the manufacturer's instruction in 384 well plates (4ti-0382;
534 4titude) format, and the LightCycler 480 PCR platform (Roche Diagnostics). Ct values above 35
535 were considered not detected, and the relative fold change in expression was calculated using the
536 delta-delta Ct method.
537
538 **Histopathology.** Tissue samples were shipped in 10% formalin solution at RT to HistoWiz Inc.
539 (US) for processing and histological examination by a certified pathologist.
540
541 **Ethics.** Samples from patients with metastatic HGSC were obtained at The Karolinska University
542 Hospital under protocols approved by The Swedish Ethical Review Agency
543 (Etikprövningsmyndigheten; 2016/119731/1, 2016/2060-32). All methods for the use of human
544 samples were carried out in accordance with relevant guidelines and regulations. Informed consent
545 was obtained from all the patients. For gastric and pancreatic cancer samples, the study has the
546 approval of the Helsinki University Hospital Ethics Committee (document number HUS 226/E6/06,
547 additional petition TMK02 § 66/2013 and HUS/1223/2021). Permission to use archive material for
548 this retrospective study without individual informed consent from the patients has been granted by
549 the Finnish National Supervisory Authority for Welfare and Health (document number
550 1004/06.01.03.01/2012) and the Finnish Medicines Agency Fimea (document number
551 FIMEA/2021/006901).
552
553 **Statistics.** *In vitro* experiments were independently performed at least three times, and at least three
554 mice per donor were compiled for *in vivo* experiments unless otherwise specified in the figure
555 legends. Data processing was performed using Microsoft Excel 2016, and graphing and statistical
556 analyses were performed using GraphPad Prism 9.0 Windows 64-bit software (San Diego, CA,
557 USA). Data are reported as mean ± standard deviation, unless otherwise specified. Statistical

558 analysis was performed using one- or two-way analysis of variance with Tukey's correction for
559 multiple comparisons and Student's *t* test, where appropriate, as indicated in the figure legends.
560 Statistical significance was set at $p < 0.05$. *p*-values are indicated in the figure legends.
561
562 **Data availability.** The data generated in this study are available upon request from corresponding
563 authors.
564
565 **Acknowledgments**
566 We thank the Laboratory Animal Center (LAC), Biomedicum Imaging Unit (BIU), Genome
567 Biology Unit (GBU) at the University of Helsinki and the Digital and Molecular Pathology Unit
568 supported by Helsinki University and Biocenter Finland for digital microscopy services for support
569 in animal care and imaging. We are also extremely grateful to Mari Rissanen, Nadezhda Zinovkina,
570 Anne Aarnio, and Sanna Vainionpää (University of Helsinki) for the valuable technical help. This
571 study was supported by CHO Pharma USA Inc. Additional funding was received from the Finnish
572 Cancer Foundation (P.M.O.), Finnish Red Cross Blood Service Research grant (P.M.O., S.L.) and
573 Sigrid Juselius Foundation (P.M.O., S.L.). E.E. was supported by the Academy of Finland
574 Postdoctoral Fellowships (no. 324487 (E.E.). These additional funders had no role in the study
575 design, data collection, interpretation or decision to submit the work for publication.
576
577 **Conflict of interest disclosure**
578 This study may lead to the development of licensed products. The authors have fully disclosed these
579 interests to EMBO Molecular Medicine journal and have an approved plan in place to manage any
580 potential conflicts arising from this arrangement. (S.L.: Beigene: Consultancy; Pfizer: Consultancy;
581 Incyte: Consultancy; Roche: Consultancy, honoraria, research funding*; Orion Pharma:
582 Consultancy; Novartis: Consultancy, honoraria, research funding*; Bayer: Research funding*;
583 Celgene: Consultancy, research funding*; Genmab: Research funding*, Gilead: Consultancy*;
584 CHO Pharma USA: Consultancy, research funding. P.M.O.: CHO Pharma USA: Consultancy,
585 research funding; Orion Corporation: CRO work*; Gertrude Biomedical Pty Ltd: CRO work and
586 research funding*. (*not related to this study).
587
588 **Funding**
589 This study was supported by CHO Pharma USA Inc. Additional funding was received from the
590 Finnish Cancer Foundation (P.M.O.), Finnish Red Cross Blood Service Research grant (P.M.O.,
591 S.L.) and Sigrid Juselius Foundation (P.M.O., S.L.). E.E. was supported by the Academy of Finland

Postdoctoral Fellowships (no. 324487 (E.E.). These additional funders had no role in the study design, data collection, interpretation, or decision to submit the work for publication.

Authors' contributions

H.J.M. and **M.H**. Conceptualization, formal analysis, validation, investigation, methodology, writing-original draft, writing-review and editing. **E.E.** Formal analysis, validation, investigation, methodology, writing-review and editing. **K.K.**, **J.W.**, **L.M-G.** and **A.R.** Resources, investigation, methodology, writing-review and editing. **T.R.J.** and **J.J.** Investigation, methodology. **P.L** and **K.L**. Resources, writing-review and editing. **H.S.**, **P.P.**, **J.W.C.**, **S.S.** and **C.H.** Resources, writing-review and editing. **P.M.O.** and **S.L.** Conceptualization, resources, formal analysis, funding acquisition, validation, writing-original draft, writing-review and editing.

References

Addeo M, Di Paola G, Verma HK, Laurino S, Russi S, Zoppoli P, Falco G, Mazzone P (2021) Gastric Cancer Stem Cells: A Glimpse on Metabolic Reprogramming. Front Oncol. 11:698394.

Alhabbab RY (2020) Targeting Cancer Stem Cells by Genetically Engineered Chimeric Antigen Receptor T Cells. *Front Genet* 11: 312

Anderson NM, Simon MC (2020) The tumor microenvironment. *Current Biology* 30: R921-R925

Askan G, Sahin IH, Chou JF, Yavas A, Capanu M, Iacobuzio-Donahue CA, Basturk O, O'Reilly EM (2021) Pancreatic cancer stem cells may define tumor stroma characteristics and recurrence patterns in pancreatic ductal adenocarcinoma. *BMC Cancer* 21: 385

Brandt LJB, Barnkob MB, Michaels YS, Heiselberg J, Barington T (2020) Emerging Approaches for Regulation and Control of CAR T Cells: A Mini Review. Front Immunol. 11:326.

Brudno JN, Kochenderfer JN (2016) Toxicities of chimeric antigen receptor T cells: recognition and management. *Blood* 127: 3321-3330

Choe JH, Watchmaker PB, Simic MS, Gilbert RD, Li AW, Krasnow NA, Downey KM, Yu W, Carrera DA, Celli A *et al* (2021) SynNotch-CAR T cells overcome challenges of specificity, heterogeneity, and persistence in treating glioblastoma. *Sci Transl Med* 13(591):eabe7378.

Cui X, Liu R, Duan L, Cao D, Zhang Q, Zhang A (2021) CAR-T therapy: Prospects in targeting cancer stem cells. *Journal of Cellular and Molecular Medicine* 25: 9891-9904

Dasyam N, George P, Weinkove R (2020) Chimeric antigen receptor T-cell therapies: Optimising the dose. *Br J Clin Pharmacol* 86: 1678-1689

635 Disis ML, Bernhard H, Jaffee EM (2009) Use of tumour-responsive T cells as cancer treatment.
636 *Lancet* 373: 673-683
637
638 Firuzi O, Che PP, El Hassouni B, Buijs M, Coppola S, Löhr M, Funel N, Heuchel R, Carnevale I,
639 Schmidt T *et al* (2019) Role of c-MET Inhibitors in Overcoming Drug Resistance in Spheroid
640 Models of Primary Human Pancreatic Cancer and Stellate Cells. Cancers (Basel). 11: 638
641
642 Green DJ, Pont M, Sather BD, Cowan AJ, Turtle CJ, Till BG, Nagengast AM, Libby EN, III,
643 Becker PS, Coffey DG *et al* (2018) Fully Human Bcma Targeted Chimeric Antigen Receptor T
644 Cells Administered in a Defined Composition Demonstrate Potency at Low Doses in Advanced
645 Stage High Risk Multiple Myeloma. *Blood* 132: 1011-1011
646 Greenbaum U, Mahadeo KM, Kebriaei P, Shpall EJ, Saini NY (2020) Chimeric Antigen Receptor
647 T-Cells in B-Acute Lymphoblastic Leukemia: State of the Art and Future Directions. Front Oncol.
648 10:1594.
649
650 Hernandez-Lopez Rogelio A, Yu W, Cabral Katelyn A, Creasey Olivia A, Lopez Pazmino Maria
651 del P, Tonai Y, De Guzman A, Mäkelä A, Saksela K, Gartner Zev J *et al* (2021) T cell circuits that
652 sense antigen density with an ultrasensitive threshold. *Science* 371: 1166-1171.
653
654 Ho M-Y, Yu AL, Yu J (2017) Glycosphingolipid dynamics in human embryonic stem cell and
655 cancer: their characterization and biomedical implications. *Glycoconjugate Journal* 34: 765-777
656
657 Jiang S, Jin J, Hao S, Yang M, Chen L, Ruan H, Xiao J, Wang W, Li Z, Yu K (2018) Low Dose of
658 Human scFv-Derived BCMA-Targeted CAR-T Cells Achieved Fast Response and High Complete
659 Remission in Patients with Relapsed/Refractory Multiple Myeloma. *Blood* 132: 960-960
660
661 Kloss CC, Condomines M, Cartellieri M, Bachmann M, Sadelain M (2013) Combinatorial antigen
662 recognition with balanced signaling promotes selective tumor eradication by engineered T cells. *Nat*
663 *Biotechnol* 31: 71-75
664
665 Lin CW, Wang YJ, Lai TY, Hsu TL, Han SY, Wu HC, Shen CN, Dang V, Chen MW, Chen LB *et*
666 *al* (2021) Homogeneous antibody and CAR-T cells with improved effector functions targeting
667 SSEA-4 glycan on pancreatic cancer. *Proc Natl Acad Sci U S A* 118
668
669 Lou Y-W, Wang P-Y, Yeh S-C, Chuang P-K, Li S-T, Wu C-Y, Khoo K-H, Hsiao M, Hsu T-L,
670 Wong C-H (2014a) Stage-specific embryonic antigen-4 as a potential therapeutic target in
671 glioblastoma multiforme and other cancers. *Proceedings of the National Academy of Sciences* 111:
672 2482
673
674 Lou YW, Wang PY, Yeh SC, Chuang PK, Li ST, Wu CY, Khoo KH, Hsiao M, Hsu TL, Wong CH
675 (2014b) Stage-specific embryonic antigen-4 as a potential therapeutic target in glioblastoma
676 multiforme and other cancers. *Proc Natl Acad Sci U S A* 111: 2482-2487
677
678 Magalhães A, Duarte HO, Reis CA (2017) Aberrant Glycosylation in Cancer: A Novel Molecular
679 Mechanism Controlling Metastasis. *Cancer Cell* 31: 733-735
680
681 Masoumi J, Jafarzadeh A, Abdolalizadeh J, Khan H, Philippe J, Mirzaei H, Mirzaei HR (2021)
682 Cancer stem cell-targeted chimeric antigen receptor (CAR)-T cell therapy: Challenges and
683 prospects. *Acta Pharmaceutica Sinica B* 11: 1721-1739
684

685 Mehta PH, Fiorenza S, Koldej RM, Jaworowski A, Ritchie DS, Quinn KM (2021) T Cell Fitness
686 and Autologous CAR T Cell Therapy in Haematologic Malignancy. *Frontiers in Immunology*
687 12:780442.
688
689 Munkley J, Elliott DJ (2016) Hallmarks of glycosylation in cancer. Oncotarget. 7(23):35478-89.
690 Newick K, O'Brien S, Moon E, Albelda SM (2017) CAR T Cell Therapy for Solid Tumors. Annu
691 Rev Med. 68:139-152.
692
693 Ochsenbein AF (2002) Principles of tumor immunosurveillance and implications for
694 immunotherapy. *Cancer Gene Therapy* 9: 1043-1055
695
696 Parte SC, Batra SK, Kakar SS (2018) Characterization of stem cell and cancer stem cell populations
697 in ovary and ovarian tumors. *J Ovarian Res* 11: 69-69
698
699 Prager BC, Xie Q, Bao S, Rich JN (2019) Cancer Stem Cells: The Architects of the Tumor
700 Ecosystem. *Cell Stem Cell* 24: 41-53
701
702 Prapa M, Chiavelli C, Golinelli G, Grisendi G, Bestagno M, Di Tinco R, Dall'Ora M, Neri G,
703 Candini O, Spano C *et al* (2021) GD2 CAR T cells against human glioblastoma. *npj Precision*
704 *Oncology* 5: 93
705
706 Rafiq S, Hackett CS, Brentjens RJ (2020) Engineering strategies to overcome the current
707 roadblocks in CAR T cell therapy. *Nature Reviews Clinical Oncology* 17: 147-167
708
709 Rodriguez-Garcia A, Palazon A, Noguera-Ortega E, Powell DJ, Guedan S (2020) CAR-T Cells Hit
710 the Tumor Microenvironment: Strategies to Overcome Tumor Escape. Front Immunol. 11:1109.
711
712 Russo D, Capolupo L, Loomba JS, Sticco L, D'Angelo G (2018) Glycosphingolipid metabolism in
713 cell fate specification. *Journal of Cell Science* 131
714
715 Schoutrop E, El-Serafi I, Poiret T, Zhao Y, Gultekin O, He R, Moyano-Galceran L, Carlson JW,
716 Lehti K, Hassan M *et al* (2021) Mesothelin-Specific CAR T Cells Target Ovarian Cancer. *Cancer*
717 *Res* 81: 3022-3035
718
719 Sigal DS, Hermel DJ, Hsu P, Pearce T (2022) The role of Globo H and SSEA-4 in the development
720 and progression of cancer, and their potential as therapeutic targets. *Future Oncol* 18: 117-134
721
722 Sivasubramaniyan K, Harichandan A, Schilbach K, Mack AF, Bedke J, Stenzl A, Kanz L,
723 Niederfellner G, Bühring H-J (2015) Expression of stage-specific embryonic antigen-4 (SSEA-4)
724 defines spontaneous loss of epithelial phenotype in human solid tumor cells. *Glycobiology* 25: 902-
725 917
726
727 Soliman C, Chua JX, Vankemmelbeke M, McIntosh RS, Guy AJ, Spendlove I, Durrant LG,
728 Ramsland PA (2020) The terminal sialic acid of stage-specific embryonic antigen-4 has a crucial
729 role in binding to a cancer-targeting antibody. *Journal of Biological Chemistry* 295: 1009-1020
730
731 Sterner RC, Sterner RM (2021) CAR-T cell therapy: current limitations and potential strategies.
732 *Blood Cancer Journal* 11: 69
733

Terraneo N, Jacob F, Dubrovska A, Grünberg J (2020) Novel Therapeutic Strategies for Ovarian Cancer Stem Cells. Front Oncol. 10:319.

Wagner J, Wickman E, DeRenzo C, Gottschalk S (2020) CAR T Cell Therapy for Solid Tumors: Bright Future or Dark Reality? *Mol Ther* 28: 2320-2339

Waldman AD, Fritz JM, Lenardo MJ (2020) A guide to cancer immunotherapy: from T cell basic science to clinical practice. *Nature Reviews Immunology* 20: 651-668

Walsh Z, Yang Y, Kohler ME (2019) Immunobiology of chimeric antigen receptor T cells and novel designs. Immunol Rev. 290(1):100-113.

Wang X, Chang W-C, Wong CW, Colcher D, Sherman M, Ostberg JR, Forman SJ, Riddell SR, Jensen MC (2011) A transgene-encoded cell surface polypeptide for selection, in vivo tracking, and ablation of engineered cells. *Blood* 118: 1255-1263

Wu JWY, Dand S, Doig L, Papenfuss AT, Scott CL, Ho G, Ooi JD (2021) T-Cell Receptor Therapy in the Treatment of Ovarian Cancer: A Mini Review. *Frontiers in immunology* 12: 672502-672502

Yamamoto TN, Kishton RJ, Restifo NP (2019) Developing neoantigen-targeted T cell–based treatments for solid tumors. *Nature Medicine* 25: 1488-1499

Zhou R, Yazdanifar M, Roy LD, Whilding LM, Gavrill A, Maher J, Mukherjee P (2019) CAR T Cells Targeting the Tumor MUC1 Glycoprotein Reduce Triple-Negative Breast Cancer Growth. *Front Immunol. 24;10:11490.*

Zhou X, Rasche L, Kortüm KM, Danhof S, Hudecek M, Einsele H (2020) Toxicities of Chimeric Antigen Receptor T Cell Therapy in Multiple Myeloma: An Overview of Experience From Clinical Trials, Pathophysiology, and Management Strategies. *Front Immunol. 23;11:620312.*

Figure legends

Figure 1. Analysis of SSEA-4 expression in tissues and cancer cell lines. A-C. SSEA-4 immunohistochemistry in (A) Ovarian, (B) pancreatic, and (C) gastric cancer patient samples. Ovarian cancer samples were also immunofluorescently stained with antibodies against SSEA-4 (red) and PAX8 (green) (A. lower panel). Representative samples are shown. **D.** Flow cytometry plots show SSEA-4 expression in human cancer cell lines. OVCAR4 (ovarian), HPAC (pancreatic) and MKN45 (gastric) were positive for SSEA-4, and Caov-3 (ovarian), MIA PaCa-2 (pancreatic) and MKN28 (gastric) were negative for SSEA-4. Unstained/isotype antibody-stained cells were used for gating the SSEA-4 negative cells.

Figure 2. Anti-SSEA-4 CAR design, T cell transduction, and CAR-T cell anti-tumor response *in vitro*. A. Schematic representation of the SSEA-4 CAR lentivector. EF1-a promoter driving the

777 expression of CSF2RA (colony stimulating factor receptor alpha 2) signal peptide followed by anti-
778 SSEA-4 V_L-(GGGGS)3-V_H scFv linked by the CD28 hinge to CD28-CD3z co-stimulatory and
779 signaling domains. EGFRt gene is located downstream and separated by the T2A self-cleaving
780 peptide. **B**. Flow cytometry plots showing percentage of transduced T cells assessed by detection of
781 EGFRt expression using cetuximab antibody. Unstained T cells were used for gating the EGFRt
782 negative cells and non-transduced (NT) T cells as a control. **C**. Quantification of transduction
783 efficiency of the cells in B. ***p=0.002*. **D**. Flow cytometry plots showing the proportion of
784 $CD4^+/CD8^+$ T cells in the cultures 8 days post transduction. Unstained/isotype T cells were used for
785 gating the CD4/CD8 negative cells and NT-T as a control. **E**. Quantification of the $CD4^+/CD8^+$
786 quantification of the cells in D. **F.** *In vitro* cytotoxicity assays using co-cultures of SSEA-4 CAR-T,
787 NT-T, and anti-GFP CAR-T cells at the indicated doses with SSEA-4^+ (left panel; OVCAR4,
788 HPAC, MKN45) and SSEA-4^- (Caov-3, MIA PaCa-2 and MKN28; right panel) cancer cells for 72
789 h. Cancer cell killing efficacy was assessed by luminescence emission from the cancer cells, and is
790 represented on the y-axis as the percentage of cell viability relative to untreated (E:T, effector :
791 target cell ratio = 0) cultures. N=3. Mean ± SD. One-way ANOVA with Tukey's multiple
792 comparison tests. (**F**) * Indicates significant differences with T cell dose = 0. ***p=0.0001; *p≤0.03*.
793 Not significant, n.s., differences were attributed to *p≥0.05.*
794
795 **Figure 3. Characterization of anti-SSEA-4 CAR-T cells *in vitro*. A.** Flow cytometry histograms
796 of CFSE (Carboxyfluorescein succinimidyl ester) cell proliferation assays showing CAR-T cell
797 proliferation upon interaction with SSEA-4^+ OVCAR4 cells in contrast to SSEA-4^- Caov-3 after 48
798 h. NT-T cells showed no proliferation in OVCAR4 and Caov-3 co-cultures. **B** and **C**. CFSE
799 quantification of cells in A. **D** and **E**. Levels of IFNγ (**D**) and IL-2 (**E**) detected by ELISA from the
800 supernatants of OVCAR4 +/- NT-T or SSEA-4 CAR-T cells at 72 h. **F**. Antibody-dependent
801 cellular cytotoxicity (ADCC) assay. SSEA-4 CAR-T cells were co-cultured with or without Natural
802 Killer (NK) cells and Cetuximab antibody at the indicated concentrations. Quantification of SSEA-
803 4 CAR-T cells was performed by flow cytometry using Protein L staining. (**B** and **C**) N=2. (**D-F**)
804 N=3. Mean ± SD. One-way ANOVA with Tukey's multiple comparison tests. (**B**) **p=0.019;* (**D-F**)
805 ****p=0.0001* and ****p=0.001*. Not significant differences, n.s., were attributed to *p≥ 0.05*.
806
807 **Figure 4. Anti-tumor response and survival in *in vivo* study. A-D**. Short-term anti-tumor
808 response of SSEA-4 CAR-T cells in NSG mice implanted intraperitoneally with $2x10^6$ FLuc-
809 expressing OVCAR4 cells. (**A**) Representative BLI images of mice treated with 1M, 2M and 3M T
810 cell doses at the indicated time points (days; d). **B-D**. BLI kinetics in the mice treated with SSEA-4

811 CAR-T at the indicated doses and compared to NT-T cells and PBS. N=5 for PBS, 2M and 3M
812 groups. N=2 for NT-T 1M group. N=3 for 1M CAR-T group. Mean ± SD. One-way ANOVA with
813 Tukey's multiple comparison tests. (**B**) ***p=0.0018* and ****p=0.0004,* (**C**) ****p=0.0009,* (**D**)
814 *****p=0.0001.* **E** and **F**. Long-term assay anti-tumor response of SSEA-4 CAR-T cells in NSG
815 mice**.** (**E** and **F**) BLI kinetics in the mice treated with SSEA-4 CAR-T at the indicated doses and
816 compared to NT-T cells and PBS. N=10 for all groups, except for NT-T 1M dose N=8. (**E**)
817 *****p=0.0001 and **p=0.0035,* (**F**) *****p=0.0001* and ****p=0.0004.* **G** and **H.** Quantification of
818 IFNγ and TNFα using ELISA in the post-mortem mouse blood plasma samples of the long-term
819 assay. N=10, except for control group (N=4), NT-T 1M (N=8), and CAR-T 1M group (N=9). **I**.
820 Probability of survival for PBS and CAR/NT-T dose mice groups after 70-day treatment.
821 ($M=1x10^6$).
822
823 **Supplementary Figure S1. SSEA-4 staining specificity and sensitivity to xylene. A.** SSEA-4
824 immunohistochemistry in paraffin-embedded gastric cancer tumor microarrays. **B**. Upper panel
825 sections were treated with standard xylene/ethanol series used in paraffin embedded section
826 treatment, whereas lower panel samples were untreated. **C**. Consecutive sections of fresh frozen
827 pancreatic cancer patient samples were stained with anti-SSEA-4 antibody. The staining was
828 blocked with SSEA-4 hexaose (middle panel) or SSEA-3 (right panel). **D.** Representative
829 immunofluorescence micrographs of SSEA-4 (red) in OVCAR-4 cells (high expression) and Caov-
830 3 cells (no expression). Nucleus (blue; Hoechst 33342). N=3.
831
832 **Supplementary Figure S2. Short-term *in vivo* study, dose-response, and weight monitoring. A**.
833 Treatment groups and used T cell doses. **B**. Weight monitoring in the indicated mice groups. CAR-
834 T 3M treated mice showed a trend of mild weight loss. ($M=1x10^6$).
835
836 **Supplementary Figure S3. IFNγ measurement and organ BLI of the short-term *in vivo* study.**
837 **A.** IFNγ quantification by ELISA in post-mortem mouse blood plasma. **B**. Representative BLI
838 images of isolated organs from mice treated with PBS, NT-T, and CAR-T cells at the indicated T
839 cell doses after 32 days. **C**. Organ BLI quantification. N=5 for PBS, 2M and 3M groups. N=2 for
840 NT-T 1M group. N=3 for 1M CAR-T group. Mean ± SD. One-way ANOVA with Tukey's multiple
841 comparison tests. (**A**) ****p=0.0005,* *****p=0.0001*. (**C**) **p=0.04,* **$p \leq 0.001$* to PBS group. Not
842 significant, n.s., differences were attributed to $p \geq 0.05$. ($M=1x10^6$).
843

844 **Supplementary Figure S4. CAR-/NT-T cell exhaustion marker quantification in the short-**
845 **term *in vivo* study. A.** Expression of human *ACTB* gene in mouse blood cell samples measured by
846 qPCR. *huACTB* Ct values were above the detection limit (ND) in PBS samples, but below the
847 detection limit in CAR-T treated mice samples at the indicated doses. **B**. Expression of human *TIM-*
848 *3*, *LAG-3,* and *PD-1* genes in blood samples of PBS-treated mice measured by qPCR. Mouse
849 *Gapdh* was used as positive control. Ct values for human *TIM-3*, *LAG-3,* and *PD-1*were above the
850 detection limit. **C**. Expression of human *TIM-3*, *LAG-3,* and *PD-1* genes in blood samples of CAR-
851 T treated mice at the indicated cell doses measured by qPCR. **D-F**. *TIM-3*, *LAG-3,* and *PD-1* fold
852 gene expression in samples of CAR-T treated mice at the indicated CAR-T cell doses. N=3. Mean ±
853 SD. One-way ANOVA with Tukey's multiple comparison tests. (**A**) ****$p=0.0078$, ****$p=0.0001$.
854 (**D**) *$p=0.0281$, ***$p=0.0001$, ****$p=0.0001$. (**E**) **$p=0.004$**.** (**F**) **$p=0.082$, ****$p=0.0001$. No
855 significant differences were attributed to $p\geq0.05$. (M=1x10^6).
856
857 **Supplementary Figure S5. Anti-tumor response and survival in the long-term *in vivo* study. A.**
858 Treatment groups and used T cell doses. **B**. Representative BLI images of mice treated with PBS,
859 1M, and 2M NT or CAR T cells doses at the indicated time points (days; d). (M=1x10^6).
860
861 **Supplementary Figure S6. Weight monitoring during the long-term *in vivo* study.** Mice treated
862 with 2M CAR-T dose showed pronounced weight loss and health deterioration at earlier time points
863 than mice treated with 1M CAR-T dose. PBS, tumor-free CAR/NT-T, and NT-T groups did not
864 show weight loss and remained healthy during the duration of the experiment. Unless otherwise
865 indicated, mice groups are tumor-bearing. (M=1x10^6).
866
867 **Supplementary Figure S7. Expression of SSEA-4 in normal mouse tissues.**
868 Immunofluorescence detection of SSEA-4 (green) in the indicated tissues of healthy 10 weeks old
869 (C57BL/6) mouse using anti-SSEA-4 antibody.
870
871 **Supplementary Figure S8. Histopathological analysis of mice after long-term *in vivo* study**
872 **treated with 2M dose. A.** H&E staining of mouse tissues from CAR/NT-T treated mice shows
873 prominent lymphocyte infiltrates in the CAR-T treated mice lungs. (M=1x10^6). **B.** CD3- and
874 EGFR-positive CAR-T cells in tissues after long-term survival study. Indicated tissues were stained
875 with HOECHST 33342 for nuclei (blue), anti-EGFR to detect CAR-T cells (middle panel; green)
876 and anti-CD3 for T cells (right panel, white). Left panel shows merged image showing all three

877 channels. Arrows highlight CAR-T and CD3 positive cells, whereas arrowheads highlight
878 erythrocytes with intense background staining.

Figure 1.

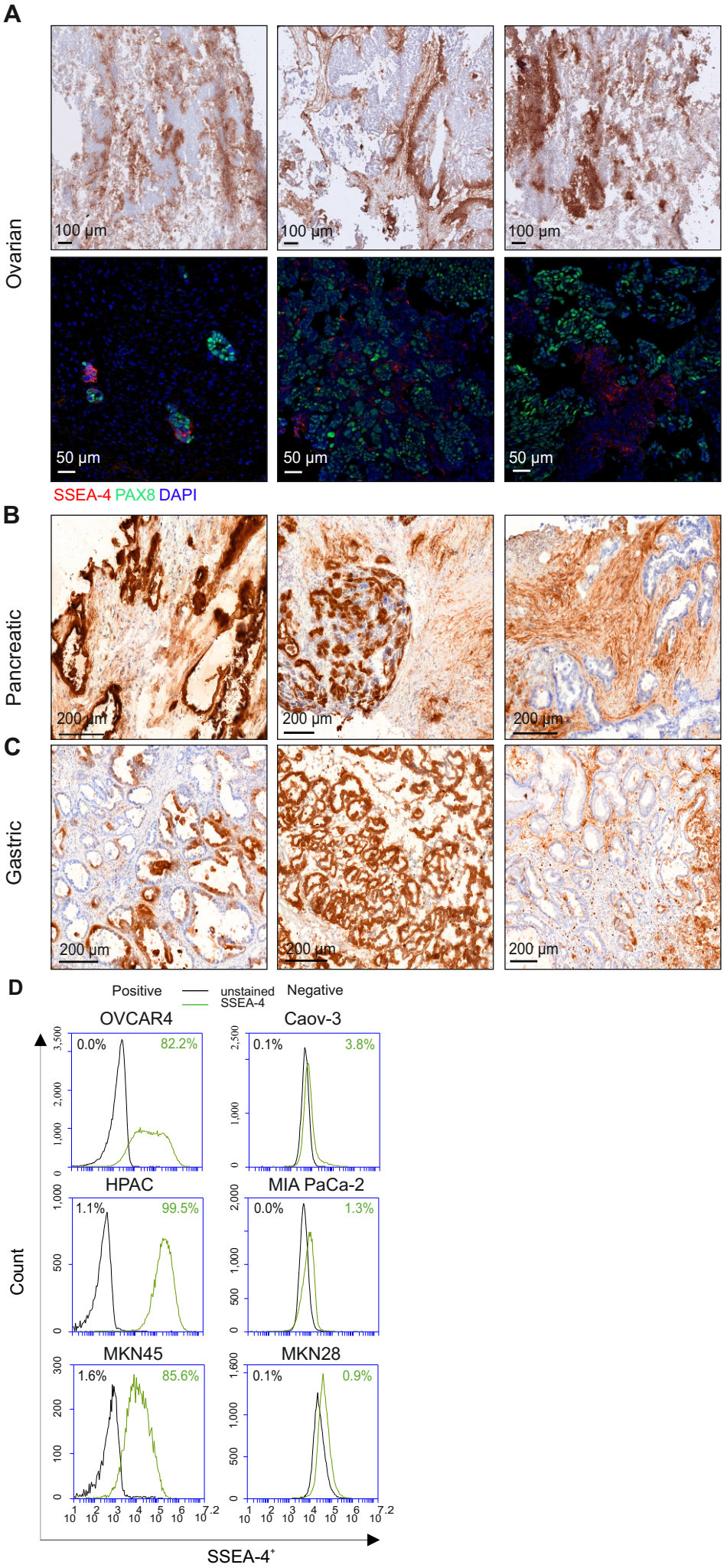
A
Ovarian
100 µm
100 µm
100 µm
50 µm
50 µm
50 µm
SSEA-4 PAX8 DAPI
B
Pancreatic
200 µm
200 µm
200 µm
C
Gastric
200 µm
200 µm
200 µm
D
Positive
unstained
SSEA-4
Negative
OVCAR4
0.0%
82.2%
Caov-3
0.1%
3.8%
HPAC
1.1%
99.5%
MIA PaCa-2
0.0%
1.3%
MKN45
1.6%
85.6%
MKN28
0.1%
0.9%
Count
SSEA-4+

Figure 2.

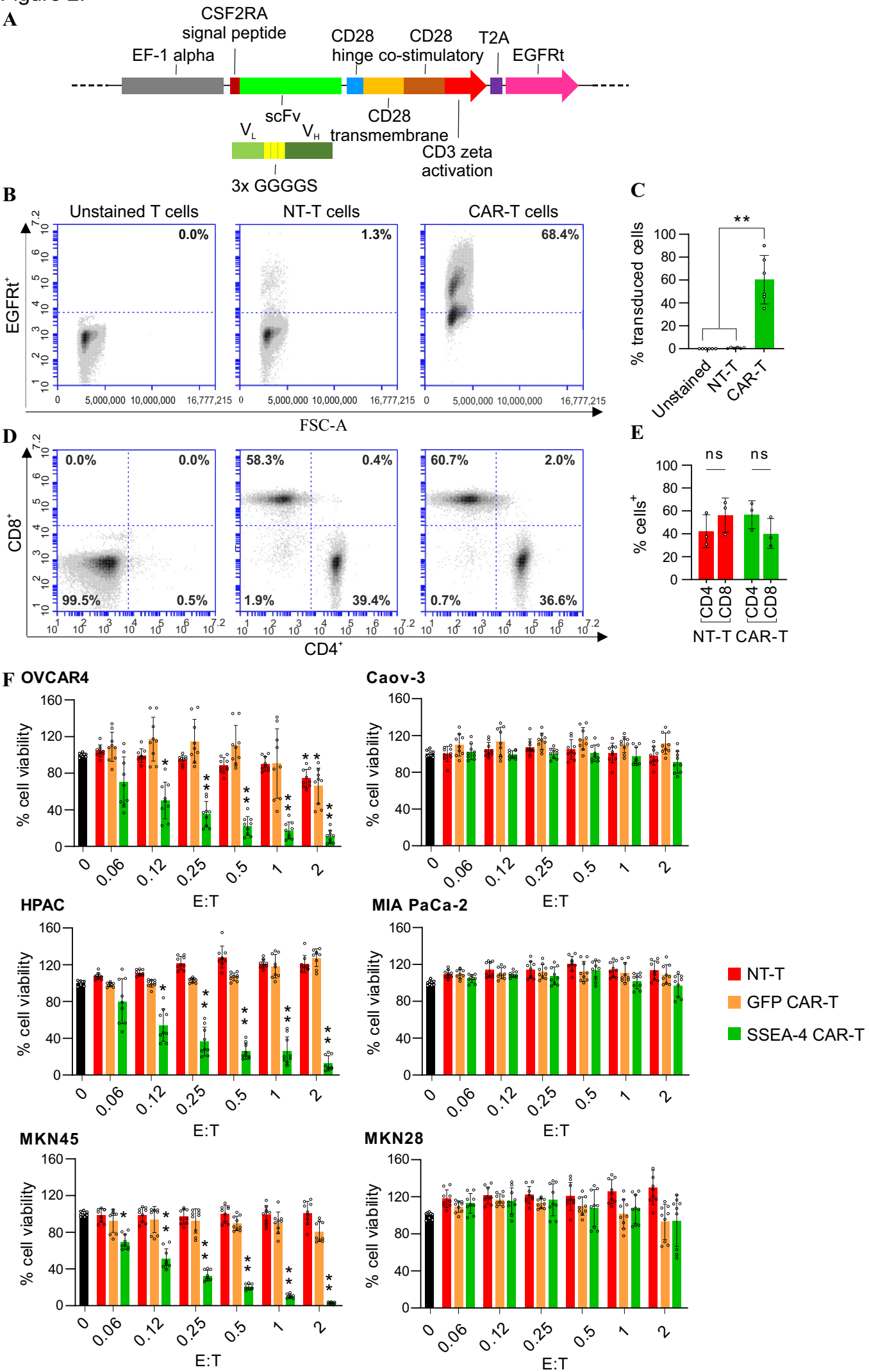
A
CSF2RA signal peptide
EF-1 alpha
CD28 hinge
CD28 co-stimulatory
T2A
EGFRt
scFv
V_L
V_H
CD28 transmembrane
CD3 zeta activation
3x GGGGS
B
Unstained T cells
NT-T cells
CAR-T cells
0.0%
1.3%
68.4%
EGFRt+
FSC-A
C
% transduced cells
Unstained
NT-T
CAR-T
D
0.0%
0.0%
58.3%
0.4%
60.7%
2.0%
99.5%
0.5%
1.9%
39.4%
0.7%
36.6%
CD8+
CD4+
E
ns
ns
% cells+
CD4
CD8
NT-T CAR-T
F OVCAR4
Caov-3
HPAC
MIA PaCa-2
MKN45
MKN28
% cell viability
E:T
NT-T
GFP CAR-T
SSEA-4 CAR-T

Figure 3.

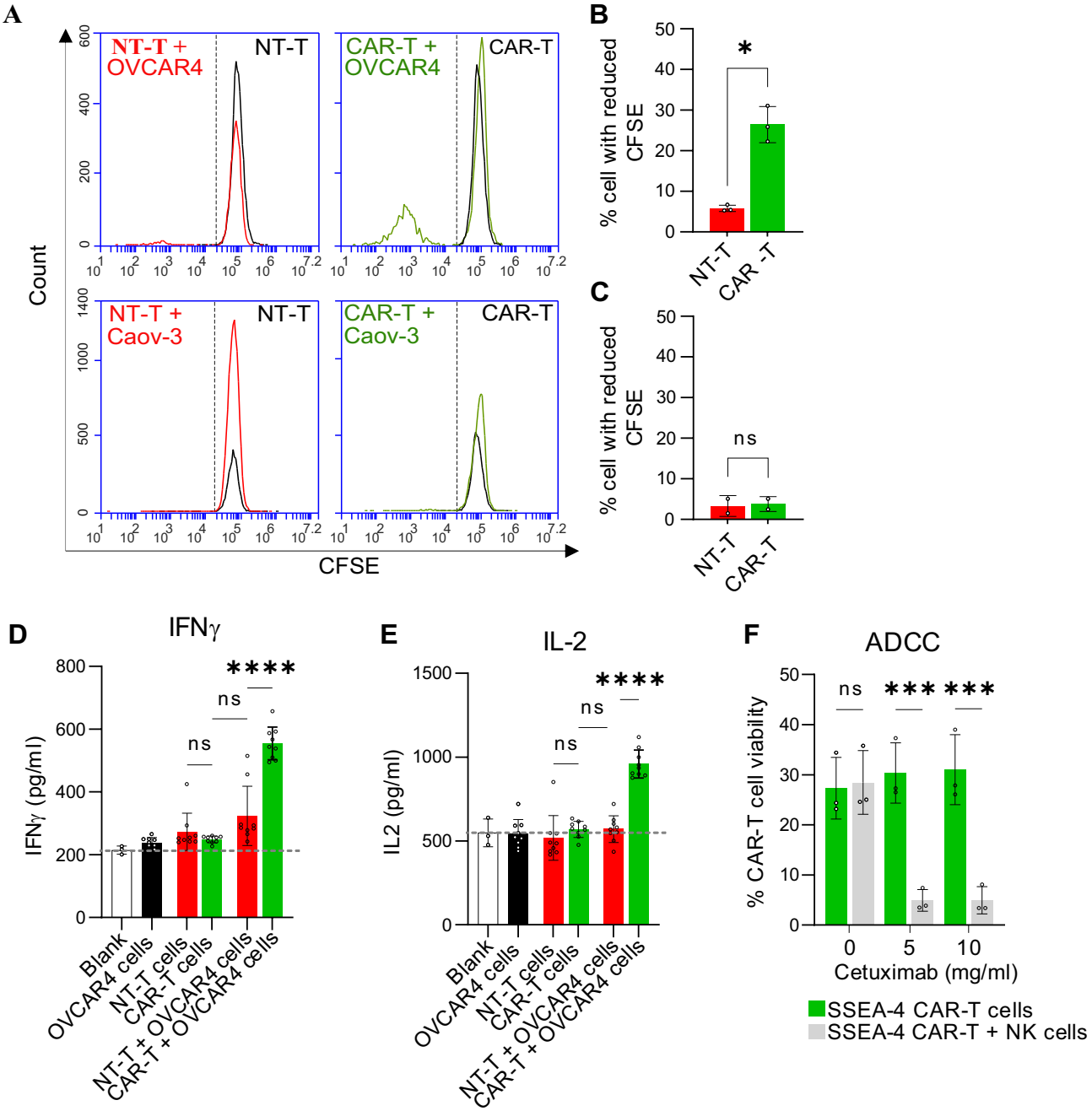
A
NT-T + OVCAR4
NT-T
CAR-T + OVCAR4
CAR-T
NT-T + Caov-3
NT-T
CAR-T + Caov-3
CAR-T
Count
CFSE
B
% cell with reduced CFSE
*
NT-T
CAR -T
C
% cell with reduced CFSE
ns
NT-T
CAR-T
D
IFNγ
IFNγ (pg/ml)
ns
ns
****
Blank
OVCAR4 cells
NT-T cells
CAR-T cells
NT-T + OVCAR4 cells
CAR-T + OVCAR4 cells
E
IL-2
IL2 (pg/ml)
ns
ns
****
Blank
OVCAR4 cells
NT-T cells
CAR-T cells
NT-T + OVCAR4 cells
CAR-T + OVCAR4 cells
F
ADCC
% CAR-T cell viability
ns
***
***
Cetuximab (mg/ml)
SSEA-4 CAR-T cells
SSEA-4 CAR-T + NK cells

Figure 4

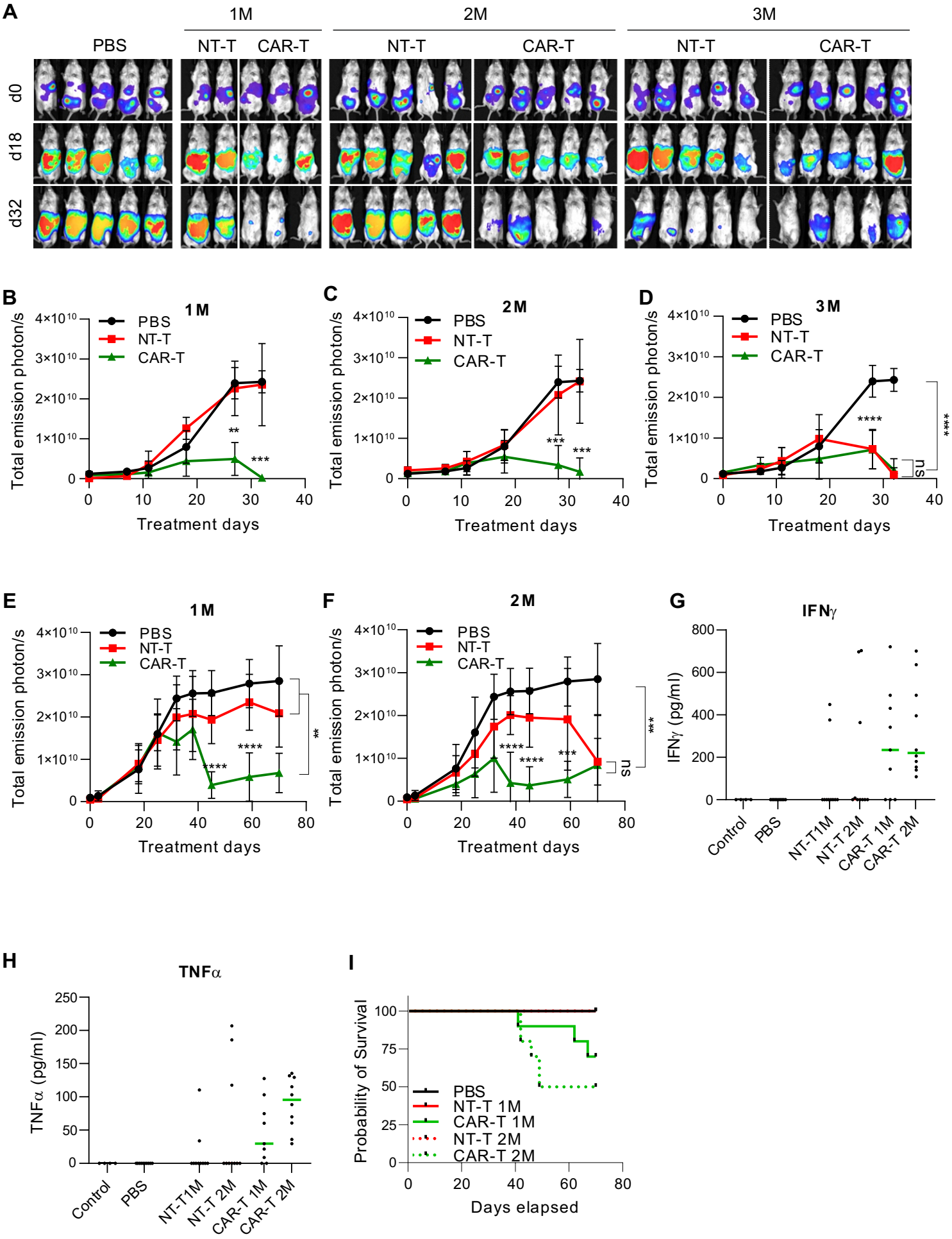
A
1M
2M
3M
PBS
NT-T
CAR-T
NT-T
CAR-T
NT-T
CAR-T
d0
d18
d32
B
1 M
C
2 M
D
3 M
Total emission photon/s
PBS
NT-T
CAR-T
Treatment days
E
1 M
F
2 M
G
IFNγ
IFNγ (pg/ml)
Control
PBS
NT-T1M
NT-T 2M
CAR-T 1M
CAR-T 2M
H
TNFα
TNFα (pg/ml)
I
Probability of Survival
PBS
NT-T 1M
CAR-T 1M
NT-T 2M
CAR-T 2M
Days elapsed